LCC-0160
Apr. 2005

Linear Collider Collaboration Tech Notes

ExB Drift of e-cloud in a PSR Quadrupole and Dipole

R. Macek
TechSource, Inc
Santa Fe, NM

M. Pivi
Stanford Linear Accelerator Center
Menlo Park, CA 94025

Abstract: In this note we will show that ExB drifts of the electron cloud in a PSR quadrupole are significant whenever the beam is present and that the longitudinal (z) motion they cause needs to be considered in constructing the various tallies that estimate electron densities and similar quantities in simulations. The effect also has important implications for generation of electron clouds in PSR and other long-bunch proton machines. In particular, one does not need significant seed electrons from grazing angle beam loss in drifts to generate a strong electron cloud in the drift space. Electrons ejected longitudinally from the quadrupoles into the drift spaces will undergo subsequent trailing edge multipactor and lead to a strong buildup.

Ex**B** Drift of e-cloud in a PSR Quadrupole and Dipole

R. Macek, TechSource, Inc., Santa Fe, NM, and
M. Pivi, SLAC, Stanford Linear Accelerator Center, Menlo Park, CA-94025.
11/3/04 draft 1, 3/28/05 draft 9

In this note we will show that ExB drifts of the electron cloud in a PSR quadrupole are significant whenever the beam is present and that the longitudinal (z) motion they cause needs to be considered in constructing the various tallies that estimate electron densities and similar quantities in simulations. The effect also has important implications for generation of electron clouds in PSR and other long-bunch proton machines. In particular, one does not need significant seed electrons from grazing angle beam loss in drifts to generate a strong electron cloud in the drift space. Electrons ejected longitudinally from the quadrupoles into the drift spaces will undergo subsequent trailing edge multipactor and lead to a strong buildup.

ExB drifts also occur in PSR dipoles but are nearly two orders of magnitude smaller. However, such drifts might still be significant after acting over a number of beam pulse passages and/or in the end fields of the dipole but are best evaluated with a suitable simulation.

Finally, we have also looked at the curvature and gradient drifts and found them to significantly smaller (by a factor of ~100) than the ExB drifts. More details on gradient and curvature drifts are given in section **IV**.

I. 2D Quad Field

Consider the case of a long-bunch, circular beam with a Gaussian distribution in the transverse coordinate, ρ, in cylindrical coordinates. If we neglect the small longitudinal (z) component of the electric field for a long bunch beam, then the 2D $\vec{\mathbf{E}}$ field in cylindrical coordinates and mks units is given by

$$\vec{\mathbf{E}} = \frac{\lambda}{2\pi\varepsilon_0}\frac{(1-e^{-\frac{\rho^2}{2\sigma^2}})}{\rho}\left(\frac{\vec{\rho}}{\rho}\right) \tag{1}$$

where λ is the line density of beam charge. The **B** field for a 2D quad is given by

$$\vec{\mathbf{B}} = g\begin{pmatrix} y \\ x \\ 0 \end{pmatrix} \tag{2}$$

where g is the quadrupole gradient. The small B field from the beam current is neglected in the following discussion.

The ExB drift velocity, $\vec{\mathbf{u}}$, (e.g. see Jackson's Electrodynamics book, 2nd edition, section 12.4) in mks units for the case in question becomes

(3) $$\vec{\mathbf{u}} = \frac{\vec{\mathbf{E}} \times \vec{\mathbf{B}}}{B^2} = \frac{\lambda}{2\pi\varepsilon_0} \frac{(1 - e^{-\frac{\rho^2}{2\sigma^2}})}{g\rho^4} \begin{pmatrix} 0 \\ 0 \\ x^2 - y^2 \end{pmatrix}.$$

On or near the coordinate axes, where much of the cloud resides when the beam is present (see Figure 1), we have: $\rho \approx x$ or y , thus

(4) $$u = \frac{\lambda}{2\pi\varepsilon_0} \frac{(1 - e^{-\frac{\rho^2}{2\sigma^2}})}{g\rho^2}.$$

The direction of the drift is given by a unit vector in the direction of $\vec{\mathbf{E}} \times \vec{\mathbf{B}}$ which is along the z axis and will be in the positive direction for electrons on or near the y axis and in the negative direction for those on or near the x axis for a PSR "D" quad (g is negative). Thus, electrons will move in both directions depending upon their location during the passage of the beam.

Animations are an informative way to present the variation in time of relevant variables resulting from simulations such as those made using e-cloud modeling code POSINST 12.1 [1], [2], [3]. Figure 1 shows a snapshot (one frame) of simulation data presented in three plots characterizing various aspects of the simulation results. The animations were constructed using the MATLAB code to process the output data of POSINST 12.1 simulations. The left dot plot is the instantaneous (x,y) distribution of macro electrons in the pipe at the peak of the 3rd bunch passage for a PSR quad. The upper right graph shows a plot of the instantaneous proton beam current, Ip in Amperes, and the "average electron line density" in the pipe as a function of time up to the frame of the snapshot. The average electron line density for the simulation shown in Figure 1 is estimated assuming that the z distribution is roughly Gaussian. The line density is computed as total number of electrons (at the time of the frame) divided by $\sqrt{2\pi} \cdot z(\text{rms})$. The units for electron line density in Figure 1 are #e's/m/2x10^7 or picoC/m/3.2. The units were chosen to keep the line density curve on the graph.

The seed electrons in the simulation for Figure 1 were generated by uniform beam losses along the 0.5 m length of the quadrupole and none outside of this region. The proton loss rate was 4.4x10^{-8}/m/proton, which is the average loss rate typical of an 8 μC/pulse beam in PSR. Also it is assumed that each lost proton produces 100 electrons which is the expectation for grazing angle beam losses. In the simulation of Figure 1, the quadrupole field is 2D and therefore has infinite extent in z, thus the ExB drift acts on all electrons whenever the beam pulse is present. The electrons spread out significantly (± 1 m or so) in z (histogram of Ze lower right graph, bin width 10 cm) each time a beam pulse passes. A more realistic model is a quadrupole field of finite length either hard edge or, better yet, a realistic 3D quadrupole model. Simulations (POSINST 12.1) with such models have been made with some results discussed in section III below.

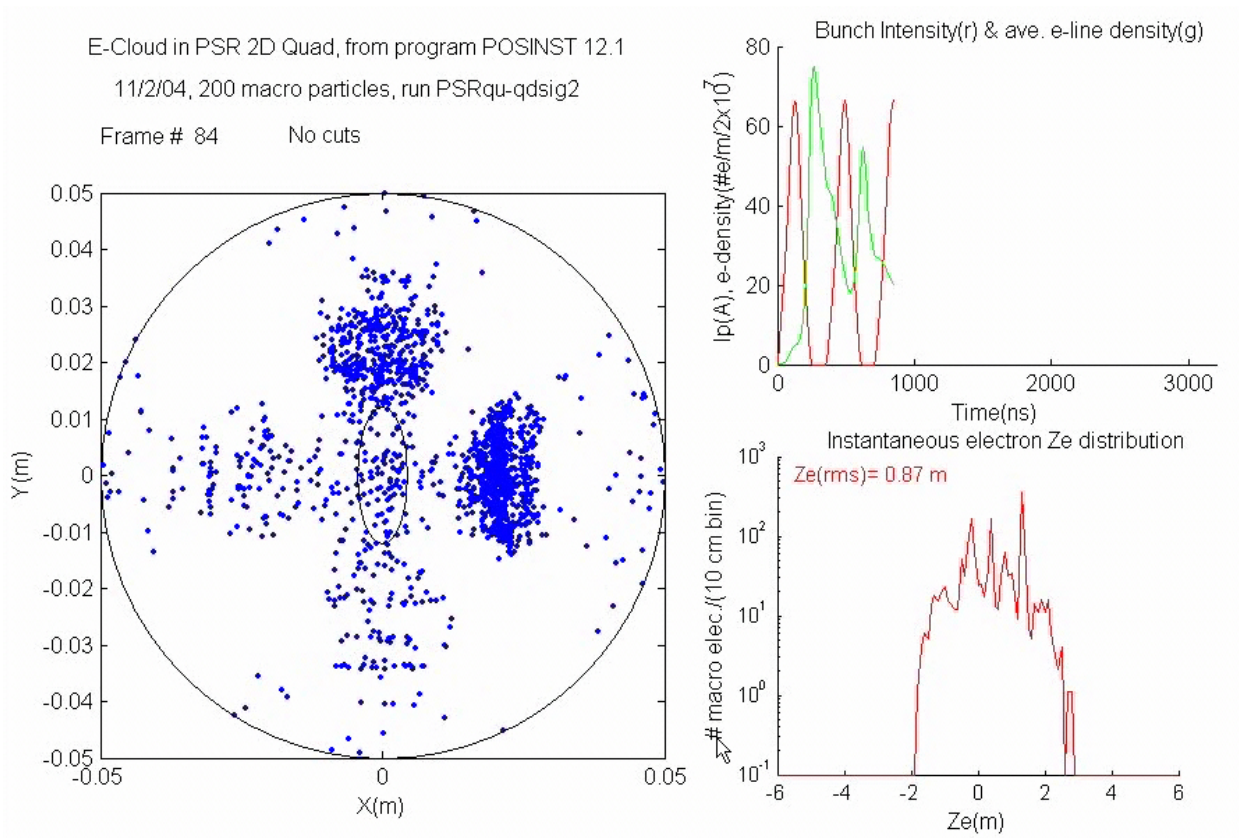

Figure 1. Snapshot (one frame with 10 ns between frames) of simulation data (POSINST 12.1) showing the distribution of electrons in the pipe at the peak of the 3rd bunch passage for a PSR "D" quad. (File: 2Dqu_Ze_dist_nocut_v2.mov, 3/12/05). The apparent lack of 4-fold quadrant symmetry in the x,y distribution in the left figure is attributed to the very limited statistics on the limited number of "seed" electrons that are generated near the peak of the bunch and thus have the highest multipacting "gain".

We will now estimate the maximum value of the drift during one passage of the beam bunch. Figure 2 shows a plot of the ρ dependence of equation 4, i.e. of $f(x=\rho\sigma) = \frac{(1-e^{-\frac{x^2}{2}})}{x^2}$.

The maximum value of u occurs at $\rho = 0$, i.e.

(5) $$u = |\vec{\mathbf{u}}| \xrightarrow[\lim \rho \to 0]{} \frac{\lambda}{4\pi\varepsilon_0 g\sigma^2}.$$

For the particular case of a PSR "D" quad and an 8 μC/pulse beam, we have g = -2.394 T/m, σ ≅ 0.01m, and the average line density during the beam pulse is 8 μC/64m = 1.25 10^{-7} C/m. For this situation, the velocity u is 4.7×10^6 m/s and the maximum drift distance during the passage of a beam pulse (time width, T=254 ns) is,

(6) $$\text{distance} = d = u \cdot T = (4.7\cdot10^6)\cdot(254\cdot10^{-9}) = \pm\ 1.19\ \text{m}$$

Note that electrons move in both + and – z directions, depending on their location in the x,y plane. The distance value above of ~1.2 m is about the size we see in the growing base-width of histograms of Ze vs time from a POSINST simulation for this case. For more information see

the animation file, 2Dqu_Ze_dist_nocut_v2.mov, 3/12/05, one frame of which is shown in Figure 1. It should also be noted that the gradient for a PSR "F" quad is 3.9 T/m and will result in a correspondingly smaller drift distance, 0.73 m, during one passage of the 8 μC beam pulse.

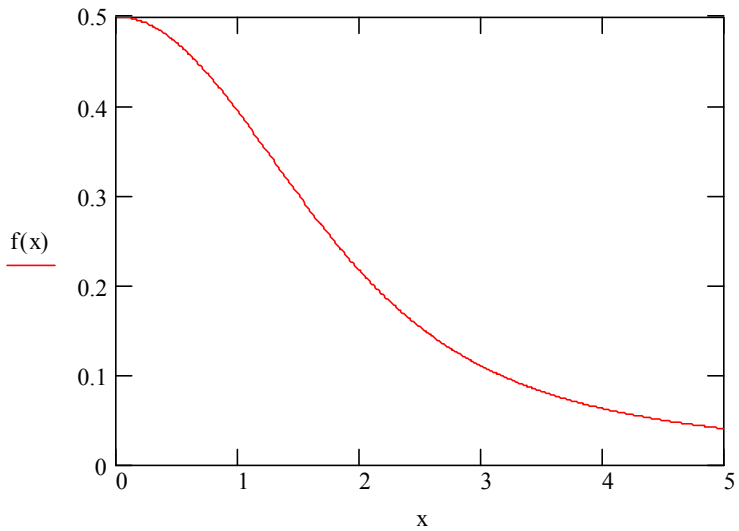

Figure 2. Graph of $f(x) = \frac{(1-e^{-\frac{x^2}{2}})}{x^2}$.

Other drift mechanisms in quadrupoles include the drifts from B field curvature and transverse B field gradient but the drifts produced are generally much smaller and will be discussed in section **IV**. However, these maybe important in some applications.

II. Dipole

On a related matter, it is of interest to look at ExB drifts in a PSR dipole. In this case,

(7) $$\vec{\mathbf{B}} = B_0 \begin{pmatrix} 0 \\ 1 \\ 0 \end{pmatrix}$$

and the drift velocity, $\vec{\mathbf{u}}$, becomes

(8) $$\vec{\mathbf{u}} = \frac{\vec{\mathbf{E}} \times \vec{\mathbf{B}}}{B^2} = \frac{\lambda}{2\pi\varepsilon_0} \frac{(1-e^{-\frac{\rho^2}{2\sigma^2}})}{\rho B_0} \begin{pmatrix} 0 \\ 0 \\ \sin(\theta) \end{pmatrix}$$

where θ is the angle between $\vec{\rho}$ and $\vec{\mathbf{B}}$. Because of the strong and constant B field (1.2 T), the drift is significantly smaller than in a quadrupole and has its maximum at θ = π/2 and ρ = 1.585σ, where the function $g(x=\rho\sigma) = \frac{(1-e^{-\frac{x^2}{2}})}{x}$ has a maximum [g(1.585)=0.451]. (See Figure 3 for a graph of g). At the maximum we have

(9) $$u_{max} = \frac{\lambda}{2\pi\varepsilon_0}\frac{0.451}{B_0\sigma}.$$

For the 8 μC/pulse beam used earlier, the maximum value of the drift distance, d_{max}, during the passage of one beam pulse is

(10) $$d_{max} = u \cdot 254\ \text{ns} = \pm\ 0.0215\ \text{m}$$

which is much smaller than the drift in a PSR quadrupole (equation (6)).

Figure 3. Graph of $g(x) = \frac{(1-e^{-\frac{x^2}{2}})}{x}$.

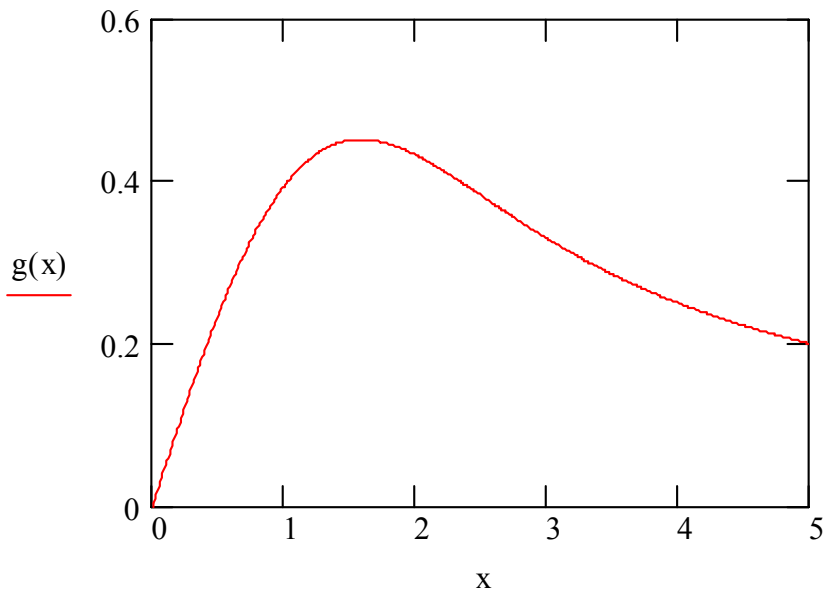

III. 3D Finite Length Quad

The PSR quadrupoles have an effective length of ~ 0.5m and a radius to the pole tip of ~ 0.090m which implies that the fringe field region is a significant fraction of the effective length. In the discussion that follows we will show that the fringe field significantly enhances the ExB motion of electrons out of the quadrupole as might be expected from equation (5) where the quadrupole gradient enters in the denominator of the expression for the drift velocity. Mauro Pivi has added a 3D model of a finite length quadrupole field with a realistic fringe field to POSINST 12.1. The 3D model is based on the Enge function as described in references [4] and [5]. Figure 4 shows a plot of the By component of the quadrupole field as a function of z.

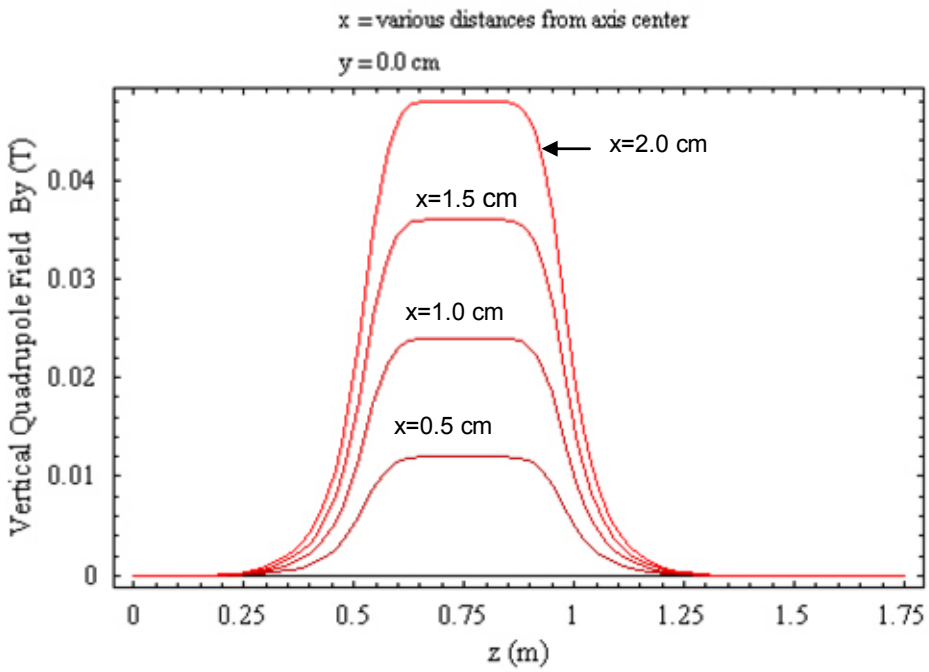

Figure 4. Plot of By in 3D model for PSR "D" quad from a Mathematica calculation by M. Pivi. Curves are shown for x=0.5, 1.0, 1.5 and 2 cm and y=0.0 cm. Quad effective length is 0.5 m and is centered at z = 0.75 m.

Simulations of electron cloud generation in a PSR "D" quad of effective length 0.5 m and gradient of -2.394 T/m have been carried out with the 3D quad model option in POSINST 12.1. In the simulation, seed electrons from proton beam losses were generated on the wall uniformly along a 0.7 m length of the quadrupole and much of its fringe field. It should be noted that no seed electrons from beam losses were generated in the drift spaces on either side of the quad but multipacting in the drift spaces can and does take place from electrons escaping the quadrupole longitudinally which are then acted upon by the space charge E field of the proton beam pulse during its passage.

Animations using pertinent output variables from the simulation are used here to show the time evolution of selected variables resulting from the simulations. Two snapshots (from file 3Dqu_Ze_dist_nocut_n.mov, 3/24/05) of simulation data showing the distribution of electrons in the pipe for the 3D quad model at two different times are shown in Figures 5 & 6. From these one sees that electrons are found 5-6 meters from the edge of the quad. In the animation one sees that they reach this distance during one passage of the beam pulse. In the x,y dot plot one is looking at the x,y projection of all macro electrons. This is a super position of electrons moving in the quadrupole field (where they tend to follow the magnetic field lines) and those moving in the drift space where the x,y motion is largely radial (for a beam centered on the axis of the pipe). It is also evident from Figure 6 that a significant number of electrons are trapped in the quadrupole well after the beam has past. Note the long, flat tail on the green curve (# of electrons) in the upper right plot of Figure 6. The effect is also seen later in Figure 17.

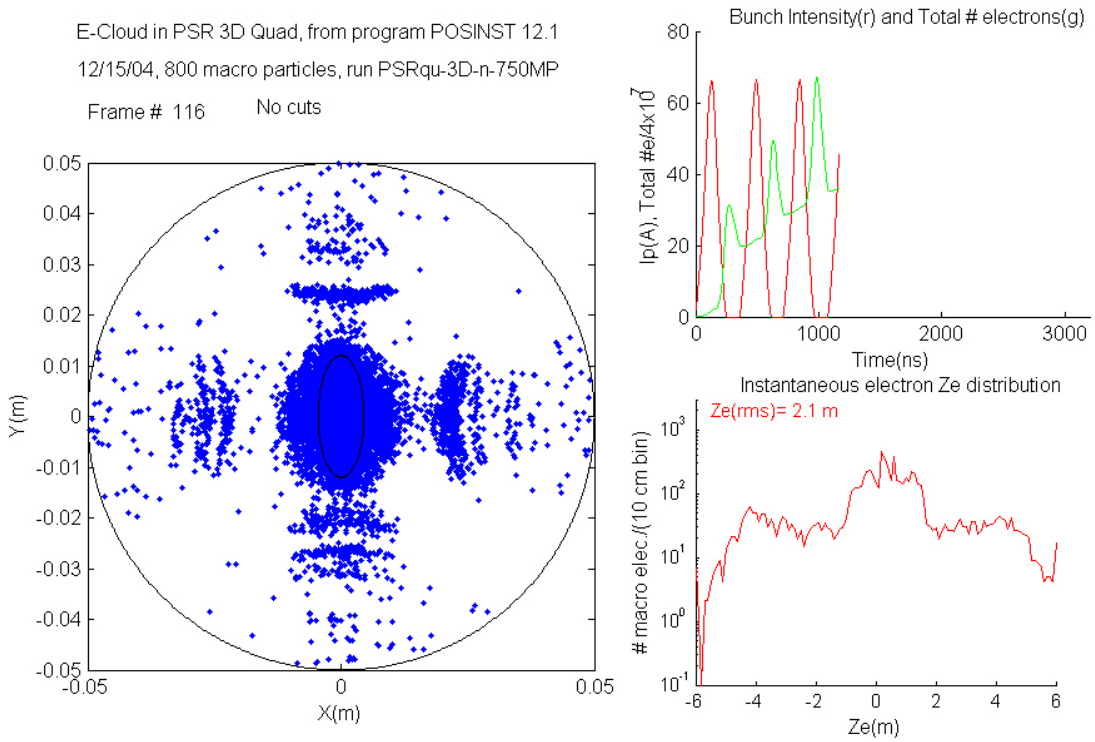

Figure 5. Snapshot (one frame) of simulation data showing the distribution of electrons in the pipe part way into the 4th bunch passage for a PSR "D" quad. Electrons are seen out as far as 5-6 meters from the edge of the quadrupole. (File: 3Dqu_Ze_dist_nocut_n.mov, 3/24/05).

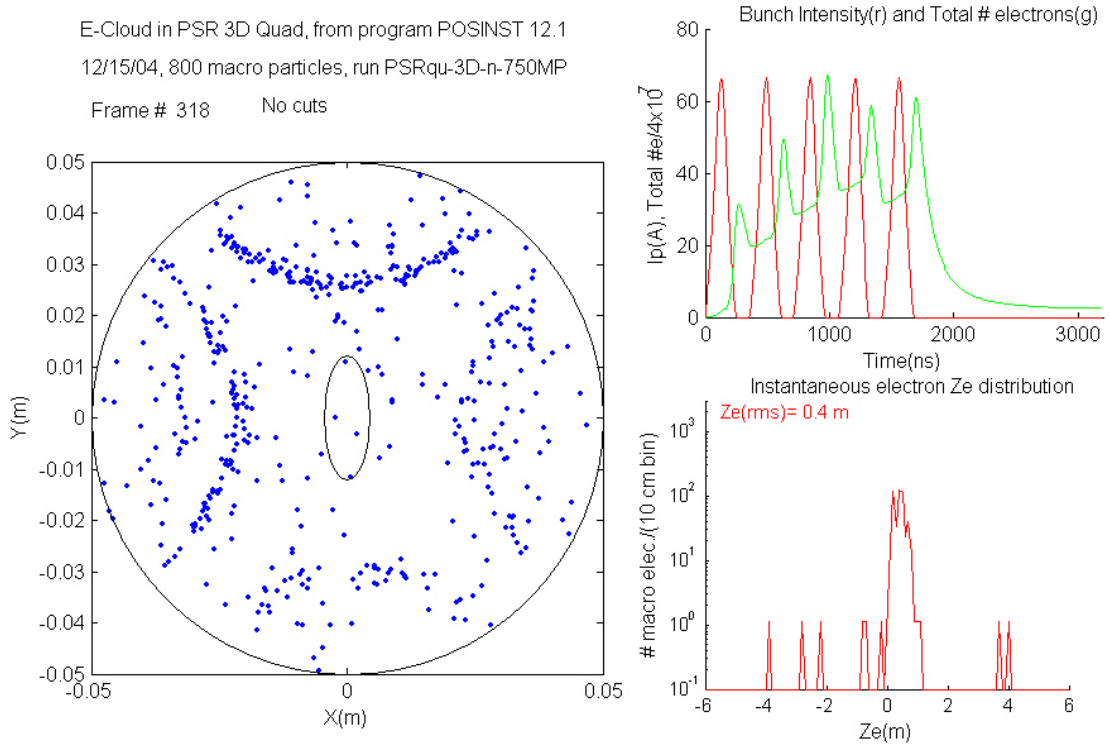

Figure 6. Snapshot showing distribution of electrons ~1.5 μs after end of 5th bunch passage. Only electrons trapped in the mirror-like fields of the quad remain. (File: 3Dqu_Ze_dist_nocut_n.mov, 3/24/05).

Other animations with cuts on the z position of the electrons provide more insights into the electron motion inside the quad (file: 3Dqu_en_dist_narrow_zcut_30cm_n.mov, 3/13/05) and in the drift space well outside the quad (file: 3Dqu_Ze_dist_z_anticut_170cm_n.mov, 3/25/05). Figures 7 & 8 are snapshots of electron distributions at two different times for those electrons with z coordinates inside the uniform gradient region of the quad (0.3 m region centered on the quad). In these plots the electrons are mostly constrained to follow the magnetic field lines of the quadrupole field. The electron energy distribution is low after the beam pulse passes (Figure 7) and is significantly higher in the middle of the beam pulse where electrons are moving under the combined influence of the space charge field of the beam and the quad magnetic fields (Figure 8).

Figures 9 & 10 show snapshots at two different times for electrons with z coordinates well outside of the quad (outside of a 1.7 m region centered on the quad). Here the electrons show the characteristics of electrons generated in a drift space i.e., radial oscillations close to the beam location when the beam is present and multipactoring on the trailing edge.

Additional insight is provided by Figures 11 and 12 where the snapshots include a dot plot of the electron z coordinate (Ze) vs the z component of velocity (v_z). At the end of the 3rd gap passage the electrons all have small v_z components (Figure 11) while at the peak of the beam pulse some electrons (ejected from the quad into the drift space) have much a much larger v_z , up to ~0.1c (Figure 12). The time evolution is much clearer in the animation than the impression one gets from a few selected snapshots (frames).

Snapshots which include the quad field region are shown in Figures 13 & 14. Figure 13 shows a z,v_z dot plot of all electrons (no z cuts) at the peak of the 5th bunch passage. This plot reveals that there is a large v_z spread in the region of the quad and just adjacent to it with electrons spreading rapidly into the drift space while the beam pulse is present. A more detailed view of the quad region and its fringe field is shown in Figure 14 where z cuts were made to select electrons with z coordinate in a 1.0 m region centered on the quad. This snapshot, taken just before the peak of the 3rd bunch, shows that many electrons in the fringe field region are acquiring a large v_z velocity component that increases rapidly as the quad field falls off. Such behavior is expected from equation (5) where the quadrupole gradient enters in the denominator of the expression for the drift velocity.

As noted earlier, the time evolution of the electron motion and distributions are much clearer in the animations than the impression one gets from a few selected frames. The various animation files each consist of 318 frames with 10 ns of elapsed time between frames. They are listed in reference [6] and are available upon request (macek@lanl.gov). Note that they are each 15 to 30 megabytes in size. They will soon be posted to the collaboration website for the PSR e-p damping experiment, http://www.sns.gov/APGroup/instability/instability.html and at the ILC electron cloud web page, http://www-project.slac.stanford.edu/ilc/testfac/ecloud/elec_cloud.html.

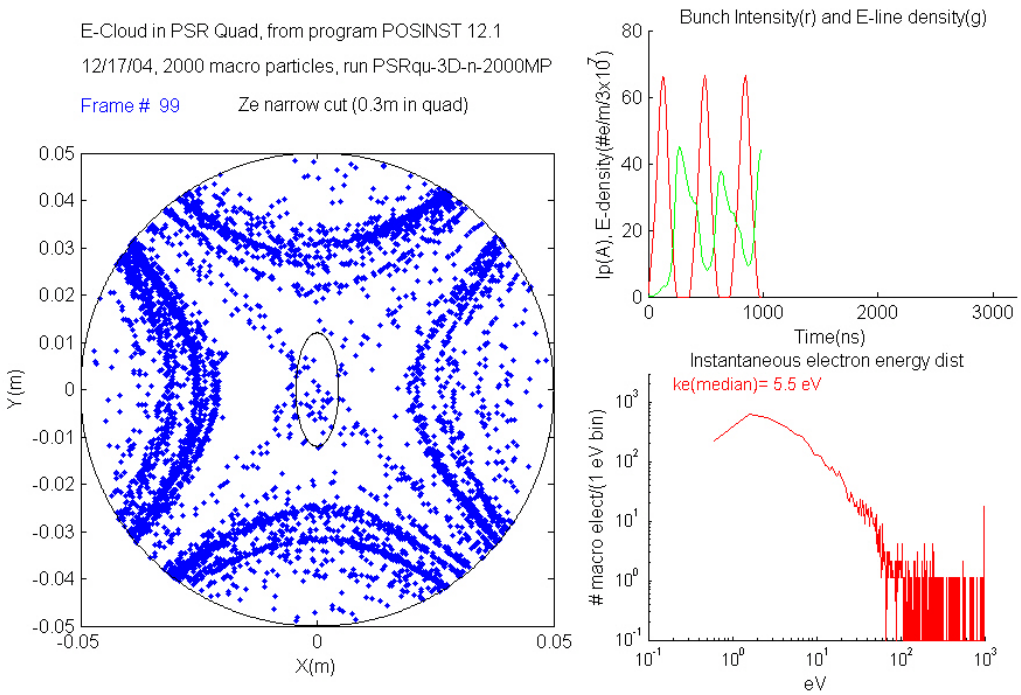

Figure 7. Snapshot showing distribution of electrons with z coordinates inside quad (0.3 m region centered on quad center) at **end** of 3rd bunch passage. The energy distribution of these electrons is shown in lower right plot. (File: 3Dqu_en_dist_zcut_30cm.mov, 3/13/05).

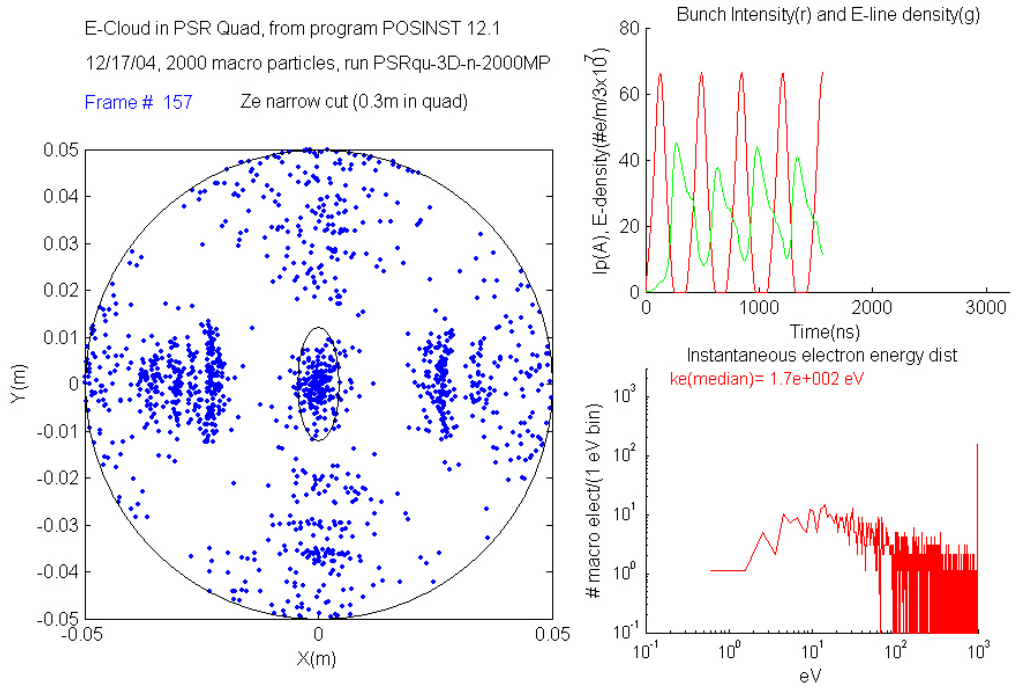

Figure 8. Snapshot showing distribution of electrons with z coordinates inside quad (0.3 m region centered on quad center) at the **peak** of 5th bunch passage. The electron energy distribution is shown in lower right plot (histogram of 1000 equal size bins but on log scale, 1 eV width, and shows a long tail out beyond 1 keV). (File: 3Dqu_en_dist_zcut_30cm_n.mov, 3/13/05).

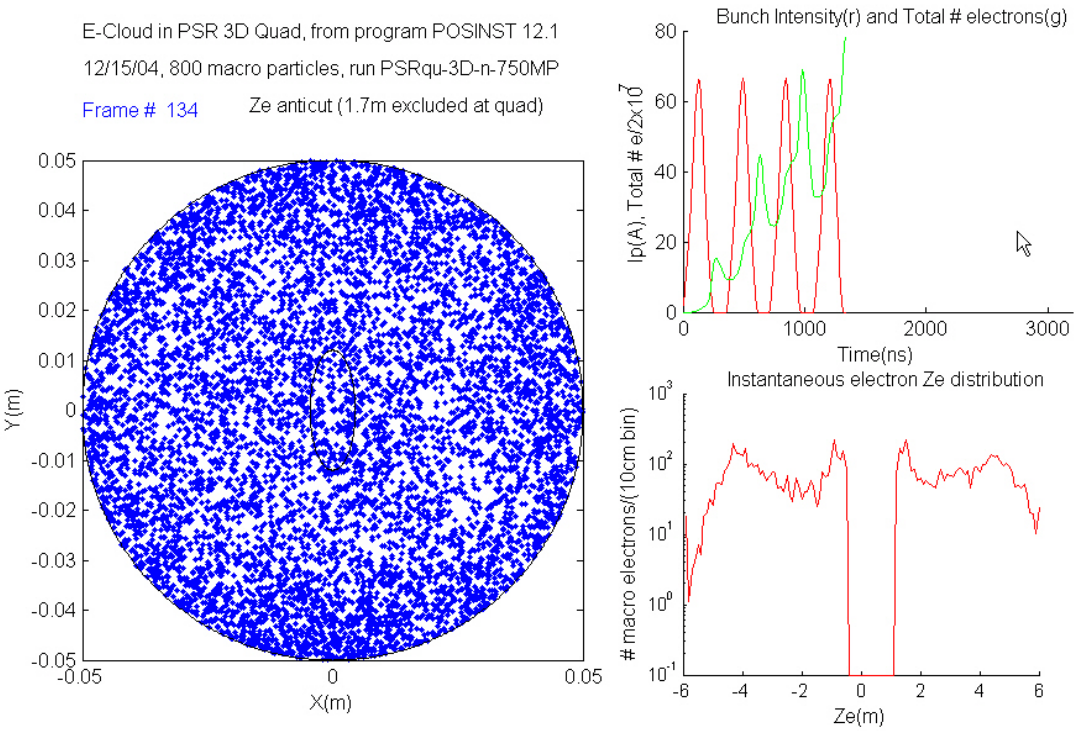

Figure 9. Animation frame showing distribution of electrons with z coordinates well outside of quad (outside of 1.7 m region centered on quad center) at end of 4th bunch passage. Figures 9 and 10 exhibit the characteristics of electrons multipacting in a drift space. (File: 3Dqu_Ze_dist_z_anticut_170cm_n.mov, 3/25/05).

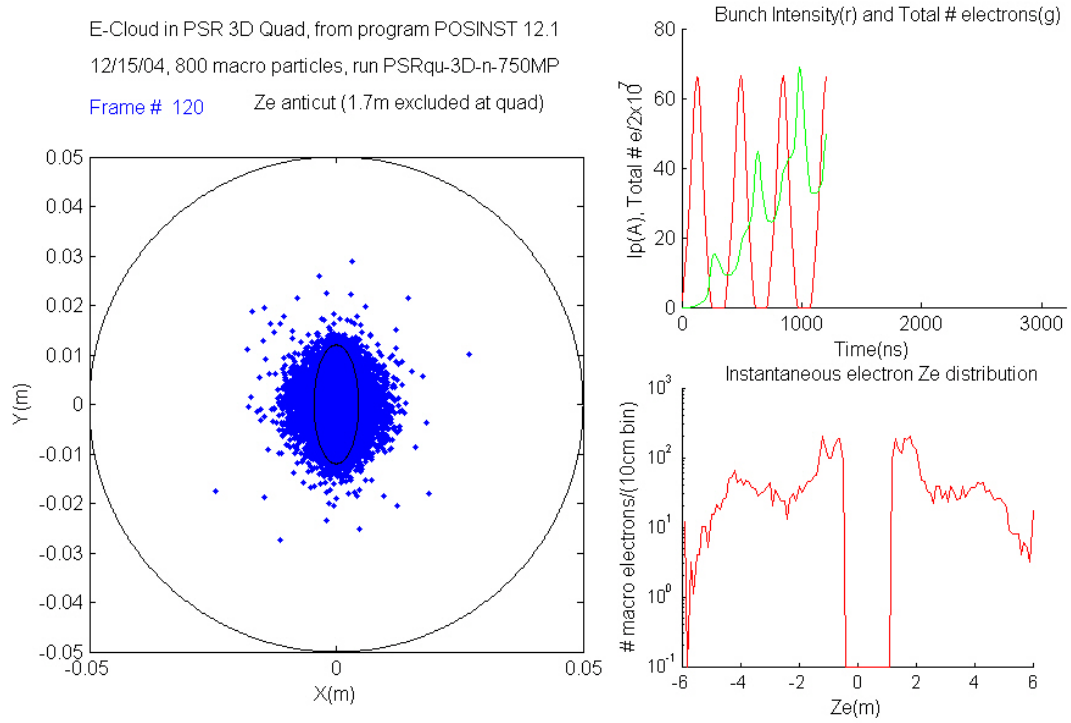

Figure 10. Animation frame showing distribution of electrons with z coordinates well outside of quad (outside of 1.7 m region centered on quad center) at the peak of 4th bunch passage. (File: 3Dqu_Ze_dist_z_anticut_170cm_n.mov, 3/25/05).

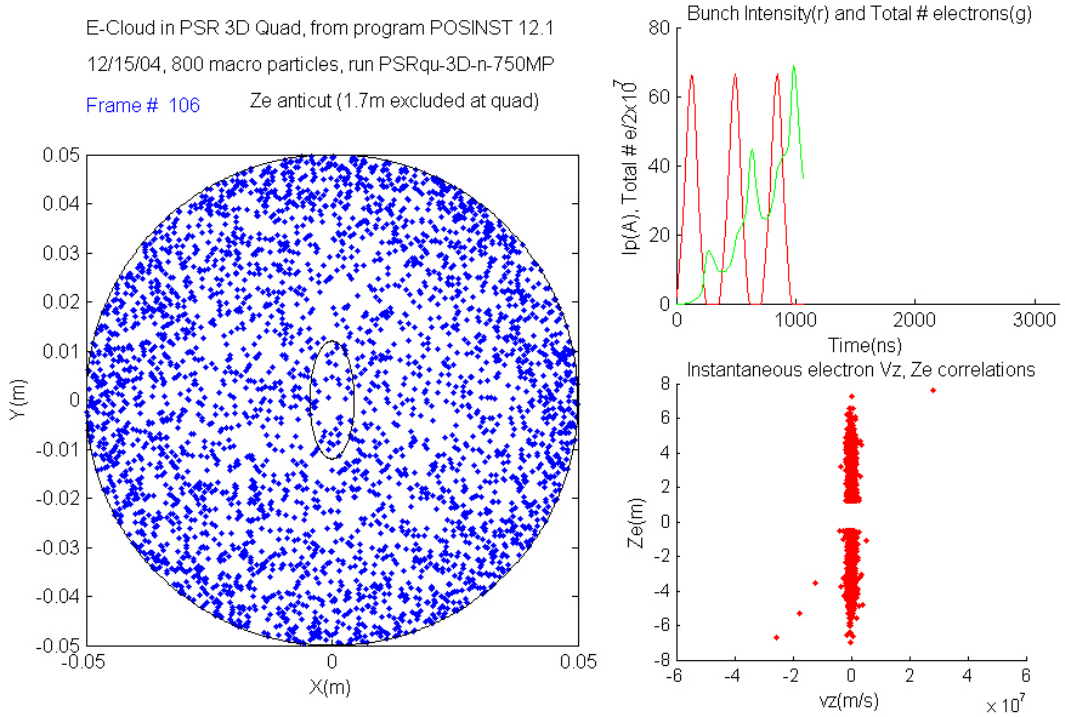

Figure 11. Snapshot showing distribution of electrons with z coordinates well outside of quad (outside of 1.7 m region centered on quad center) at the end of 3rd gap passage (near beginning of 4th bunch passage). (File: 3Dqu_Vz_Ze_cor_zanticut_170cm_n.mov, 3/25/05).

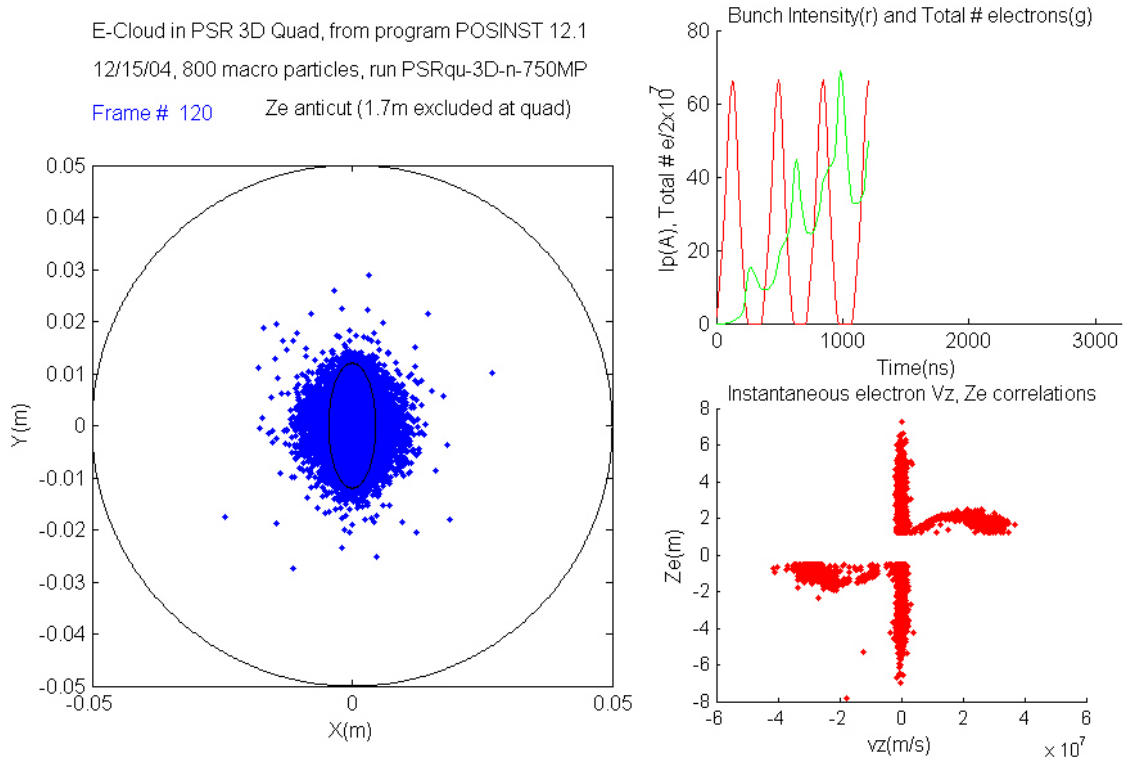

Figure 12. Snapshot showing distribution of electrons with z coordinates well outside of quad (outside of 1.7 m region centered on quad center) near the peak of the 4th gap passage. (File: 3Dqu_Vz_Ze_cor_zanticut_170cm_n.mov, 3/25/05).

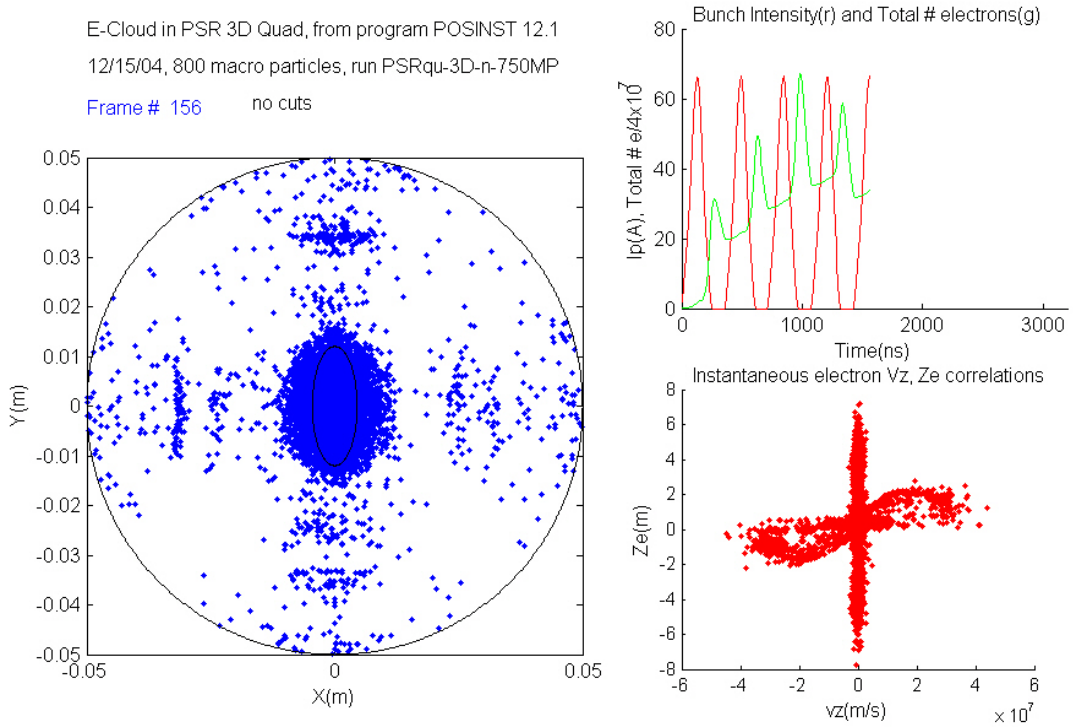

Figure 13. Snapshot showing electron distributions and v_z, z correlations with no cut on the electron z coordinates (v_z scale 10^7 m/s). (File: 3Dqu_Vz_Z_cor_nocut_n.mov, 3/25/05).

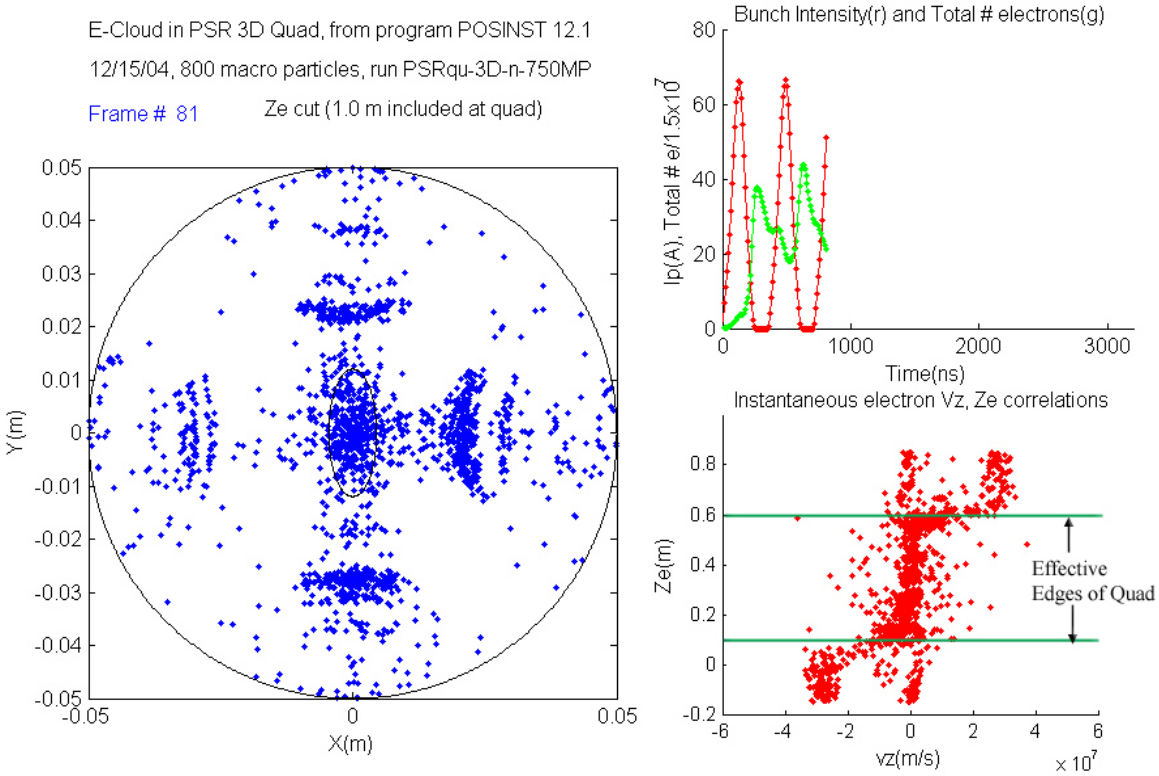

Figure 14. Snapshot showing v_z, z correlations for region of the quadrupole and fringe field (1.0 m region centered on quad). The effective edges of the quad are shown as green lines at Ze = 0.1m and 0.6 m. (File: 3Dqu_Vz_Z_cor_zcut_1m_n.mov, 3/25/05).

IV. Estimates of gradient and curvature drifts in a 2D quadrupole field

Other drifts are caused by $\nabla_\perp \mathbf{B}$ and the curvature of the B field lines. These are still present in the absence of an $\vec{\mathbf{E}}$ field from the beam. Both drifts can be combined into one formula for the drift velocity, $\vec{\mathbf{V}}_D$, (See Jackson's Electrodynamics book, 2nd edition, section 12.4):

(11) $$\vec{\mathbf{V}}_D = \frac{(v_\parallel^2 + v_\perp^2/2)}{\omega_B \cdot R}\left(\frac{\vec{\mathbf{R}} \times \vec{\mathbf{B}}}{R \cdot B}\right) = \frac{(v_\parallel^2 + v_\perp^2/2)}{v_\perp}\left(\frac{\vec{\mathbf{R}} \times \vec{\mathbf{B}}}{R \cdot B}\right)\left(\frac{a}{R}\right),$$

where $v_\parallel$ is the electron velocity component parallel to $\vec{\mathbf{B}}$, $v_\perp$ the component perpendicular to $\vec{\mathbf{B}}$, R the radius of curvature of the field lines at the location of the electron, and ω_B the electron's gyro frequency $\vec{\mathbf{B}}$ which can be written as $\frac{v_\perp}{a}$, where a is the gyro radius of the electron motion about $\vec{\mathbf{B}}$.

The static 2D quadrupole magnetic field can be obtained from a magnetic scalar potential [real part of a complex potential $W(z) = -i\frac{g}{2}z^2 = gxy + i\frac{g}{2}(y^2 - x^2) = \phi + i\psi$],

(12) $$\phi(x,y) = \mathrm{Re}(W(z)) = gxy.$$

Likewise the field lines are given by lines of constant $\psi(x,y)$ (the stream function):

(13) $$\psi(x,y) = \mathrm{Im}(W(z)) = \frac{g}{2}(y^2 - x^2).$$

The radius of curvature vector, $\vec{\mathbf{R}}$, from the center of curvature to the plane curve of $\psi(x,y) =$ constant is given by [7]

(14) $$\vec{\mathbf{R}} = \begin{pmatrix} 1 + \left(\frac{dy}{dx}\right)^2 \\ \frac{d^2y}{dx^2} \end{pmatrix}\begin{pmatrix} -\frac{dy}{dx} \\ 1 \\ 0 \end{pmatrix} \text{ and the magnitude } R(x,y) = \frac{(x^2+y^2)^{3/2}}{(y^2-x^2)}$$

The derivatives of y with respect to x were obtained by differentiating (13) with respect to x. Using (2) for $\vec{\mathbf{B}}$ and (14) for $\vec{\mathbf{R}}$ and after some manipulation we find

(15) $$\left(\frac{\vec{\mathbf{R}} \times \vec{\mathbf{B}}}{R \cdot B}\right) = -\vec{\mathbf{k}}, \text{ where } \vec{\mathbf{k}} \text{ is the unit vector along the longitudinal z axis.}$$

Combining (15) and (11) we obtain

$$\vec{\mathbf{V}}_D = -\vec{\mathbf{k}}\frac{(v_\parallel^2 + v_\perp^2/2)}{v_\perp}\left(\frac{a}{R}\right). \tag{16}$$

The quantity a/R is generally quite small and the drifts produced are small compared to the ExB drifts when beam is present. We have calculated the combined gradient and curvature drift for the electrons in one of the simulations (shown in Figure 7 and 8) and generated an animation showing the distribution of V_D at various times in the simulation. Figure 15 is a frame at the peak of the passage of the 5 beam pulse in which the lower right graph is a histogram of the Vd distribution. This frame has the distribution of V_D with the largest base width in this sequence. The higher values of V_D are due to electrons near the origin (larger R) and more energetic electrons (higher velocity). Other frames presented in Figure 16 (at the end of the 3rd beam pulse) and Figure 17 (at the end of the sequence) show very narrow distributions of V_D, which result from the smaller energy distribution and absence of electrons at the origin.

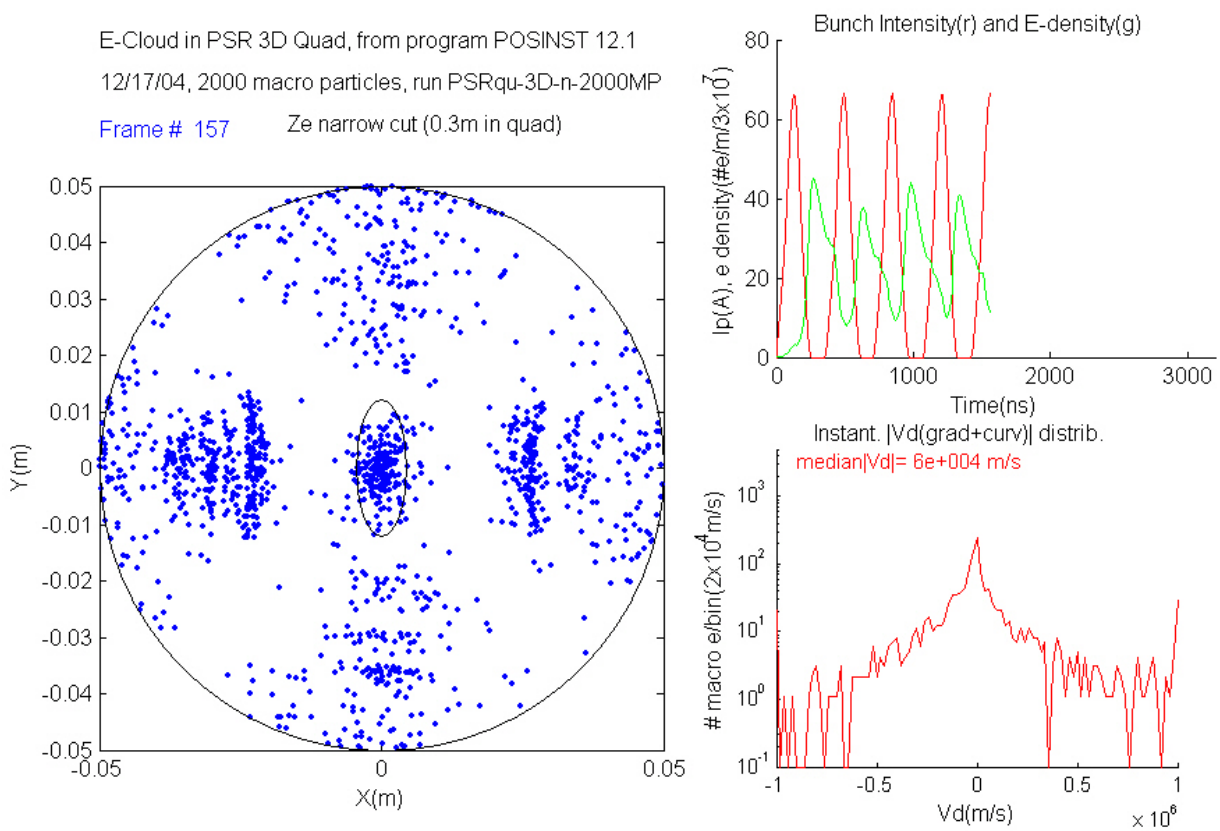

Figure 15. This animation frame shows the distribution of drift velocity, V_D, (in the lower right graph, V_D scale is 10^6 m/s) due to gradient and curvature effects in a PSR quad. The time of the frame corresponds to the peak of the 5th bunch passage. Electrons were selected with z coordinates inside a 0.3 m region centered on the quadrupole. (File: 3Dqu_Vd_dist_zcut_30cm_n.mov, 3/25/05).

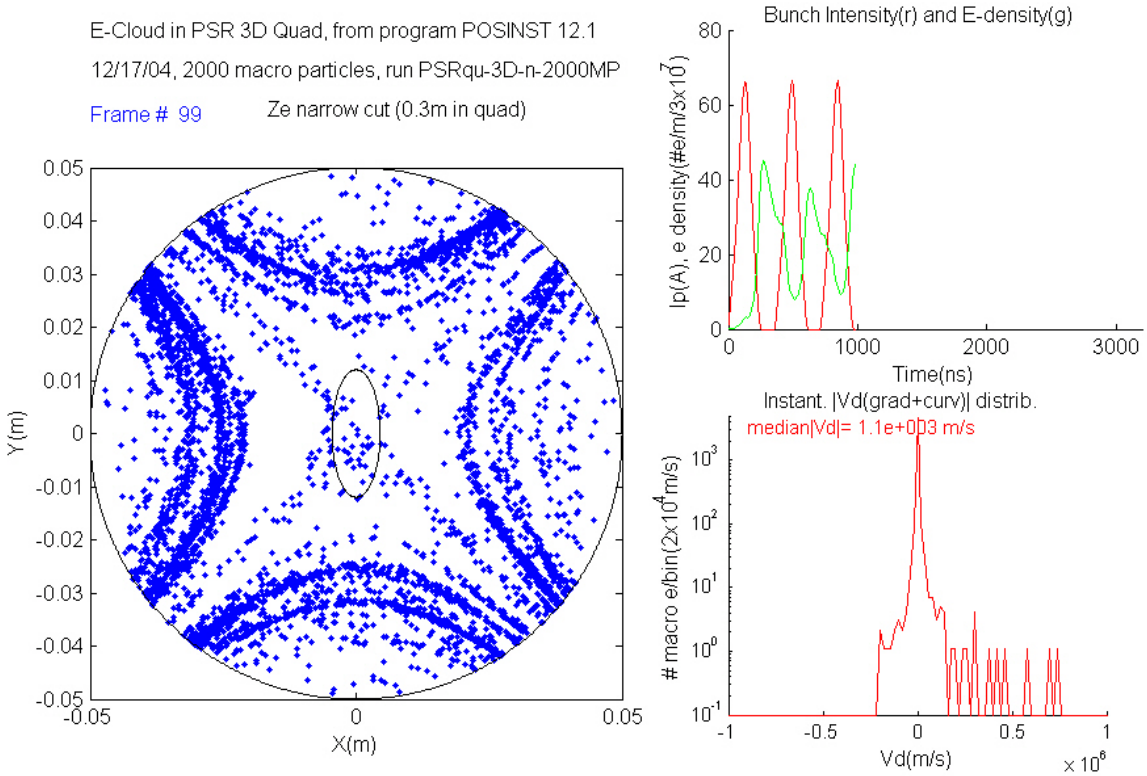

Figure 16. Animation frame showing a narrow distribution of V_D at the end of the third beam bunch passage. (File: 3Dqu_Vd_dist_zcut_30cm_n.mov, 3/25/05).

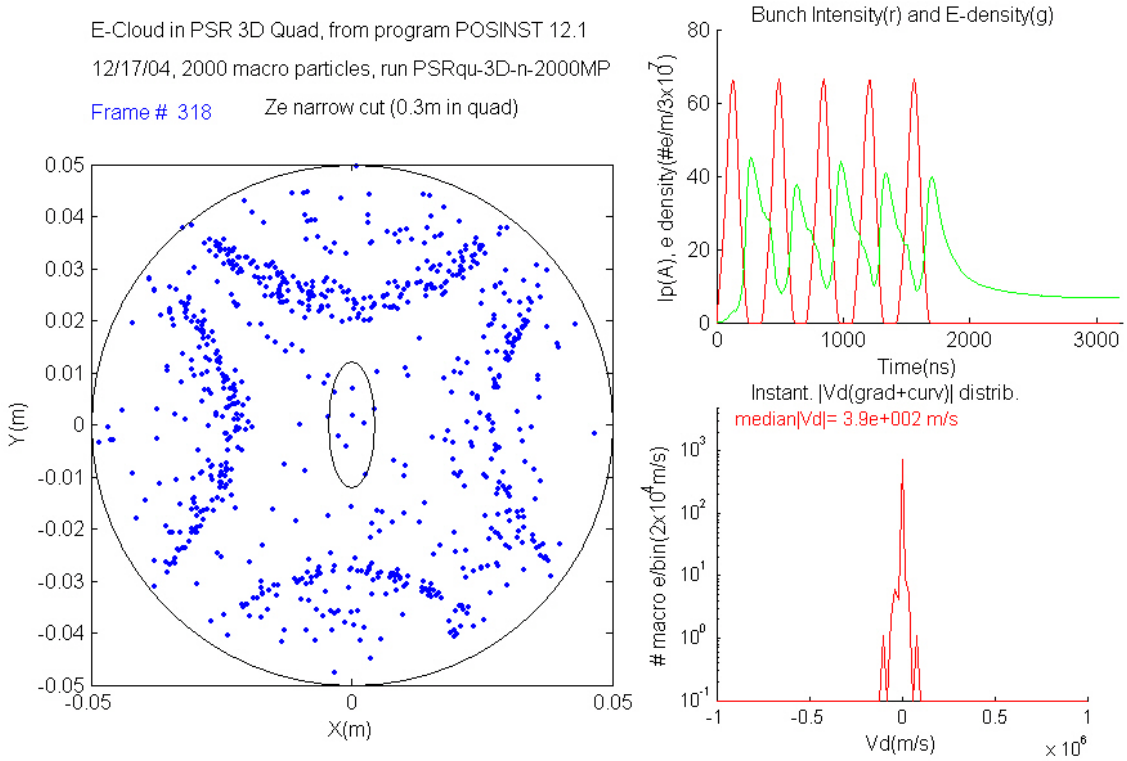

Figure 17. Animation frame showing the very narrow distribution of V_D electrons ~ 1.5 μs after the end of the last beam bunch. (File: 3Dqu_Vd_dist_zcut_30cm_n.mov, 3/25/05).

V. Some preliminary conclusions and speculations

The simulations described here show that numerous electrons generated by trailing edge multipactor in quadrupoles (for a long beam bunch) can acquire significant longitudinal velocities (z component) and be ejected into drift regions beyond the quadrupole. Analytical models indicate that this is caused by an ExB drift mechanism that is most pronounced for electrons which are pulled into small radii during the bunch passage. The electrons ejected into the drift space can be further amplified by trailing edge multipactor in the drift space. Drifts due to $\nabla_{\perp}\mathbf{B}$ and the curvature of the B field lines were found to be quite small (less than 1%) compared with maximum drift from ExB effects.

These results suggest that many of the electrons observed in drift spaces may come from electrons ejected from nearby quadrupoles and are further amplified by trailing edge multipactor in the drift space. Other simulations show that multipactor of seed electrons born at the wall from beam losses in the drift spaces does not result in electrons with sizeable v_z components.

The electrons ejected from the quads into drifts spaces may explain why we have seen so many electrons in drifts spaces such as section 4 of PSR where we would not expect many seed electrons from grazing angle beam losses. The major losses in PSR come from large angle coulomb scattering in the foil and should be lost in the quads where the beta functions are largest. From our understanding of beam losses at PSR, it does not seem likely that beam scattered from the quad would make many grazing angle collisions with the vacuum chamber surfaces in drift spaces. To resolve this more conclusively it would be possible, in principle, to develop a code (or modify an existing code) to track beam losses and the resulting scattered radiation. In addition, it should be possible to develop diagnostics to measure the electrons generated in quads as well as those trapped in the quads.

It may also be possible to design experiments to observe the electrons being ejected from the quadrupoles. For example, one might give the beam a single turn kick (kicker in section 3) to increase the losses and then observe the time it takes the electrons to increase in the drift space in section 4.

Acknowledgements

Robert Macek would like to thank Miguel Furman for all of his help, guidance and training given him in the use of POSINST. We would also like to thank T. O. Raubenheimer for many useful discussions and the support of the project.

The work by R. Macek was primarily supported by a DOE Phase I SBIR grant (DE-FG02-04ER84105) and was immeasurably aided by the hospitality of LANSCE division at LANL where R. Macek, as a guest scientist, has access to PSR and its beam physicists.

References

[1] M. A. Furman and G. R. Lambertson, "The Electron cloud Instability in the Arcs of the PEP-II Positron Ring," LBNL-41123/CBP Note-246, PEP-II AP Note AP 97.27, 1997. also Proc. Intl. Workshop on Multibunch Instabilities in Future Electron and Positron Accelerators (MBI-97),

KEK, Tsukuba, Japan, 15-18 July 1997, KEK Proceedings 97-17, Dec. 1997 (Y. H. Chin, ed.), p.170.

[2] M. A. Furman, "The Electron-Cloud Effect in the Arcs of the LHC", LBNL-41482/CBP Note 247/LHC Project Report 180, May 20, 1998.

[3] M. A. Furman and M. T. F. Pivi, "Probabilistic Model for the Simulation of Secondary Electron Emission", LBNL-49771/CBP Note-415, November 6, 2002; PRST-AB paper v5/i12/e124404 (2003).

[4] M. Berz, B. Erdelyi and K. Makino, "Fringe field effects in small rings of large acceptance", Physical Review Special Topic Volume 3,124001 (2000)

[5] G. Bowden, "Fringe field representation of IP magnet", ABC Technical Note #046, 9/26/1991, available at http://ccdb3fs.kek.jp/cgi-bin/img_index?9203240

[6] Animation files mention in this report.

File Name	Date last modified	Figure #	Page
2Dqu_Ze_dist_nocut_v2.mov	3/12/05	1	3
3Dqu_Ze_dist_nocut_n.mov	3/24/05	5,6	7
3Dqu_en_dist_zcut_30cm_n.mov	3/13/05	7,8	9
3Dqu_Ze_dist_z_anticut_170cm_n.mov	3/25/05	9,10	10
3Dqu_Vz_Ze_cor_zanticut_170cm_n.mov	3/25/05	11,12	11
3Dqu_Vz_Ze_cor_nocut_n.mov	3/25/05	13	12
3Dqu_Vz_Ze_cor_zcut_1m_n.mov	3/25/05	14	12
3Dqu_Vd_dist_zcut_30cm_n.mov	3/25/05	15-17	14-15

[7] G. Born and T Korn, "Mathematical Handbook for Scientists and Engineers", McGraw-Hill, 1961. Section 17.1-4, p 499-500.